2.2 Experimental Description

2.2.1 The Rheo-Fluidification Processor

In a Rheo-Fluidification processor, a melt extrudes continuously through treatment zones where it is submitted to a combination of shear-thinning and strain-softening via the use of cross-lateral shear vibration superposed to pressure flow (originated by an extruder feed). Figure 2.1 shows two treatment stations – (11) and (22) – for a melt flowing from left to right to exit at the end of the processor, where its viscosity is measured continuously by an in-line rheometer and it is water cooled, granulated into pellets.

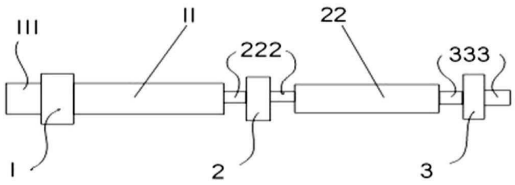

Figure 2.1 Schematic of a Rheo-Fluidizer with two stations

The "treatment" in stations (11) and (22) is sketched in Figure 2.2: the melt flows through (from left to right) a gap, "3", where the upper gap surface is static and the lower surface is rotated and (optionally) oscillated. Both surfaces contain small ribs, "12", detailed in Figure 2.3 and Figure 2.4, which create local vibrational extensional flow by squeezing and un-squeezing the melt as it is being swept forward helicoidally.

Shear-thinning is controlled by the shear rates, which add up vectorially from all types of flow (longitudinal and cross-lateral, vibratory or not), and strain softening is controlled by frequency and the strain amplitude of the cross-lateral shear component. The rotation of the rotor in station 1 and station 2 were in opposite directions, a situation that we casually called "comb to the left–comb to the right", referring to the sweeping induced by the ribs in relation to the rotation direction.

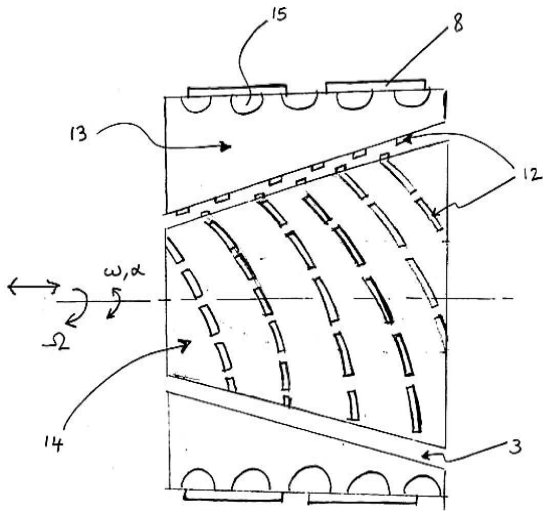

Figure 2.2 Details of the "inside" of one station in Figure 2.1

2.2.2 Sustained-Orientation

Figure 2.5 shows the viscosity of the exiting melt (PMMA) just after it has been "treated", i.e., at the end of the second station of the two-station Rheo-Fluidizer shown in Figure 2.1.

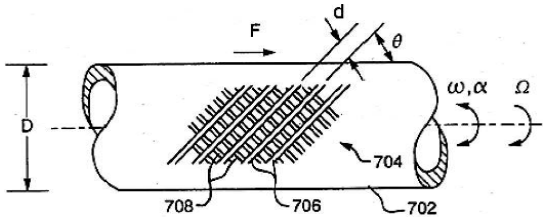

Figure 2.3 The surfaces touching the melt have a network of "ribs" to induce vibration as the melt passes through

perature, frequency sweep tests show a gradual return to a normal pseudo-plasticity and Newtonian viscosity.

Table 2.1 Flow Improvement for Pellets Showing Sustained Orientation

	Virgin MFI	MFI after "treatment" (and correction for M_w change)	Flow improvement (%)
Polycarbonate	12	21	75
PETG	8	12	50
LLDPE	0.5	1.2	140
Polystyrene	4	6	50
PMMA	17	37	118

2.4 Discussion

Our research has two goals: (1) a theoretical, fundamental understanding of the stability of the network of entanglement and (2) a practical goal: how Rheo-Fluidification proceeds by way of "disentanglement of the chains", and how we can predict the processing parameters responsible for its triggering (temperature, strain, strain rate in both shear and extension) that will produce sustained-orientation. The theoretical objective raises fundamental questions regarding our present understanding of the interactions between the macromolecules that give rise to entanglements, these "physical cross-links". Our experiments at least suggest that the classical concept of M_e to describe entanglements is too simplistic and its usefulness is probably limited to the linear range of viscoelasticity.

The practical goal of this program will be fully achieved when we will be able to predict the processing parameters for a successful Rheo-Fluidification treatment, yielding any chosen value of sustained-orientation, given a polymer melt of known molecular weight characteristics, topology, and chemical structure. In simple terms, for a given throughput of melt flow, what should be the Rheo-Fluidification processing temperatures in the stations, the value of combined strain rate (from pressure and drag flow, oscillatory and rotational), the value of extensional flow and strain rate, the value of pressure in the gap, and what will be the amount of sustained-orientation obtained? Further, what will be the stability of the new entangled state (how fast will it re-entangle at any given temperature and pressure)? Therefore, the theoretical and fundamental part of this research is to provide a science base for molding processes under shear-thinning and strain-softening controls, so that the process result can be achieved rationally based on scientific laws rather than only on experience.

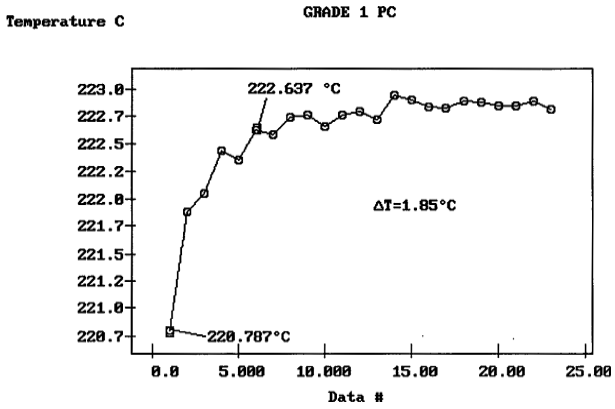

Figure 3.8 Stabilization of temperature in the rheometer oven as a function of the data point measurement (corresponding to a frequency increase).The increase of temperature of 1.85 °C corresponds to the sixth data point

In summary, it seems appropriate to warn against the use of "uncontrolled" data from various sources to test the validity of sensitive equations. "Randomness" of the residuals for alleged good fits might be artificially created by mixing data from several workers, and mistaken with the effect of thermal history, which is known to create scatter and an unacceptable level of accuracy compared to experimental errors. As already said before, it seems more appropriate to generate the data carefully, using the same protocol of sample preparation, the same procedure to test the specimen, the same instrument to determine molecular weight characteristics, the same instrument to measure the viscoelastic data, by the same operator, and especially using the same lot for the resin.

3.6 Critical Analysis of the Equations of Rheology

3.6.1 Universality of WLF Constants at T_g

The simplest myth to knock down, because it is already largely admitted, is the myth that universal constants C_{1g} and C_{2g} enter the WLF formulation of Newtonian viscosity, Eq. (3.3).

Figure 3.9 is a plot of $\mathrm{Log}(\mu_o/\mu_{og})$ vs $(T - T_g)$ for the three polycarbonate grades. The value of T_g for the respective polymers is known from PVT analysis, by inter-

cepting the rubbery and glassy volume–temperature behavior, at atmospheric pressure. The Newtonian viscosity μ_o at each temperature is obtained by fitting the non-linear behavior with the generalized Cross–Carreau equation, Eq. (3.6). For each grade, we verify that Log(μ_o) vs T can be fitted rather well (with r^2 better than 0.999) by a hyperbolic function, which can, indeed, be rewritten as a WLF equation, Eq. (3.3) [17], from which the two constants C_{1g} and C_{2g} are derived. The value of μ_{og} in Figure 3.9 and Eq. (3.3) is computed by extrapolation from the hyperbolic fit, knowing the value of T_g (see Table 3.1).

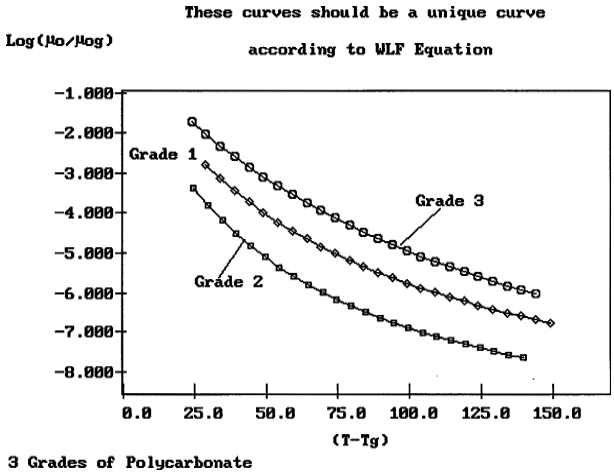

Figure 3.9 Log(μ_o/μ_{og}) vs ($T - T_g$) for PC. These three curves should be a single curve according to the WLF equation

Table 3.1 Fitting Parameters in WLF Eq. (3.3) for the Three PC Grades of Figure 3.9

	T_g (°C)	Log(μ_{og})	C_{1g}	C_{2g}
GRADE 1	136.0	9.842	10.22	76.70
GRADE 2	145.4	11.58	10.46	51.88
GRADE 3	151.0	12.06	11.87	84.16

Figure 3.9 demonstrates that plots of Log(μ_o/μ_{og}) vs ($T - T_g$) for the three polycarbonate grades do not resume to a single curve, as predicted if the WLF constants were universal [17]. The values obtained for C_{1g} and C_{2g} are convincingly different from the universal constants proposed by William, Landel, and Ferry [17], respectively 17.44 and 51.6. Also, it is observed that Log(μ_{og}) for the three grades is not equal to 13, and does not stay constant with molecular weight, even for the two linear polymers Grade 1 and 2.

Thus, based on the second conclusion, a melt can have several steady states at the same temperature and strain rate, depending on its state of entanglement, and it appears that shear can modify the entanglement state at will: this is the basis of "shear-refinement". If entanglements can be kept in an unstable state long enough, it is possible to produce "disentangled polymers" that, in terms of viscosity decrease, are attractive commercial "grades". The challenging question is how to retain in a metastable state (that we could control) the lower viscosity melt produced at the end of a transient "treatment" and then recover the original properties after processing.

Another conclusion seems to emerge from these experiments: shear-thinning might just become time dependent, under certain strain rate conditions. In other words, whatever causes shear-thinning produces a melt state that is not stable under certain conditions. The transient behavior observed would be the reflection of that time dependence of shear-thinning, and the molecular motions involved in shear-thinning and in the transient decay might be closely related, if not identical.

Figure 4.20 shows the effect of annealing the melt in the middle of a transient decay to see if the melt would reconstruct its internal structure to provide the original viscosity after annealing. The shear rate history shown in the box of Figure 4.20a was applied to the melt (the temperature was 215 °C). The difference with Figure 4.18 is that the melt was rested (un-sheared) for 30 minutes at the end of the transient decay induced by a shear rate of 1 sec^{-1}. Then the melt was sheared at a rate of 0.1 sec^{-1}. Figure 4.20b shows the variation of viscosity with time, Figure 4.20c shows the variation of normal force, and Figure 4.20d presents details of (c) around the zero normal force line. It is clear (Figure 4.20b) that the melt nearly regained its original viscosity after the time of rest when no mechanical deformation was applied. This is evidence that the equilibrium state for a strain rate of 0.1 sec^{-1} was the original viscosity. The normal force was almost zero for the initial strain rate (Figure 4.20c, left curve), went up, and decayed when the strain rate was changed to 1 sec^{-1}, and was zero for the second application of a 0.1 sec^{-1} strain rate. Zooming in on the zero line region of box (c) shows that the normal force decay during transient behavior actually converged to a small negative value (step 2 curve), but that after annealing (step 4 curve), the normal force had returned to zero.

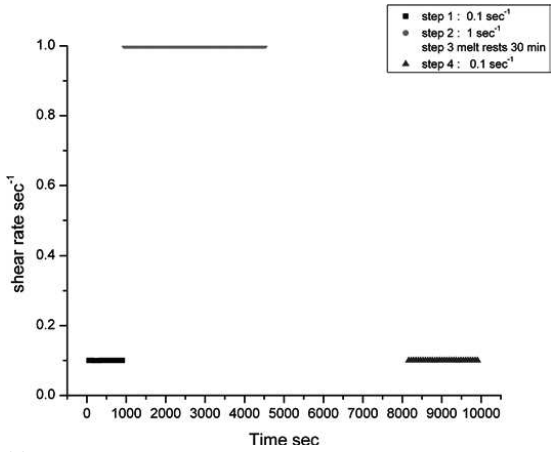
step 1 : 0.1 sec-1
step 2 : 1 sec-1
step 3 melt rests 30 min
step 4 : 0.1 sec-1
shear rate sec-1
Time sec

(a)

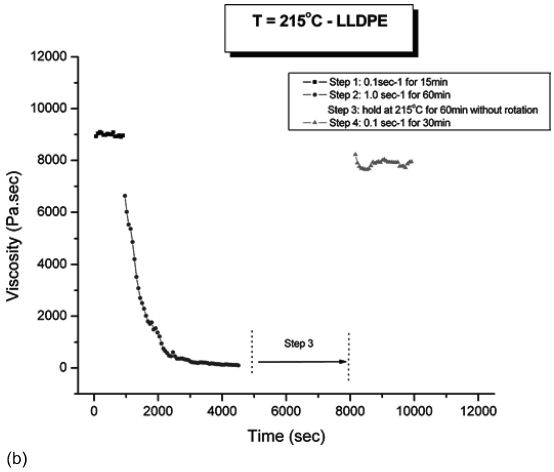
T = 215°C - LLDPE
Step 1: 0.1sec-1 for 15min
Step 2: 1.0 sec-1 for 60min
Step 3: hold at 215°C for 60min without rotation
Step 4: 0.1 sec-1 for 30min
Viscosity (Pa.sec)
Step 3
Time (sec)

(b)

scribe the data well enough to determine ω'_0 accurately. There are other empirical functions, such as a Carreau type of equation, Eq. (5.2), which could be applied to describe the relationship between ω' and ω equally well within the range of ω. Figure 5.12 demonstrates another way to find ω'_0 that, in our opinion, has much more physical significance, as will be shown later. This figure shows that ω' can be expressed as a function of G^* and that it could be fitted (for small strain) by a simple exponential growth function:

$$\omega' = \omega'_0 + A_1 \cdot \left[\exp\left(G^*/G_1^*\right) - 1\right] \tag{5.12}$$

Here, in Figure 5.12, $\omega'_0 = 34.1$; $A_1 = 58.733$; $G^*_1 = 0.0279$ MPa. Eq. (5.12) can be rewritten as:

$$Ln\left(\frac{k\omega' + (1-k)\,\omega_o'}{\omega_o'}\right) = \frac{G^*}{G_1^*}$$

$$\text{with} \qquad k = \frac{\omega_o'}{A_1} \tag{5.13}$$

In this form, a mixing formula between ω' and ω'_0 appears in the numerator of the logarithm, with compounding factor k. One can define an average ω'_{av} equal to $(k\omega' + (1-k)\omega'_0)$, with k constant in the regime of deformation described in Figure 5.12 (we will see later that k is a strong function of the strain γ). In the section dealing with the effect of strain, we identify k with the activated phase-lines coherence factor for a given ω', the $(1-k)$ non-activated (or relaxed) ones having the static frequency ω'_0. This concept that the phase-lines of the entanglement network in Figure 5.7 do not need to be strained all at once, nor all the time, implies a sequential stretch–relax mechanism, and in that sense, k can be regarded as the fraction of time an activated phase-line is stretched (with ω' a frequency defining the stretched state), while $(1-k)$ is the fraction of time it is in the static, unstressed state (characterized by ω'_0). A similar mixing rule formula will be described in a later section giving a description of shear-thinning from the point of view of the cohesive energy of the network.

When $k = 1$ in Eq. (5.13), the formula simplifies to the classical Eyring modelization of flow, Eq. (5.14), in which stress "plasticizes" the activation energy of diffusion, which we find from the temperature variation of ω'_0 (see next section):

$$\omega_o' = \omega_{oo}' \exp\left(-\frac{\Delta_{\omega'}}{RT}\right)$$

$$\omega' = \omega_{oo}' \exp\left[-\frac{\left(\Delta_{\omega'} - \left(\frac{RT}{G_1^*}\right)G^*\right)}{RT}\right] \tag{5.14}$$

where $\Delta_{\omega'}$ is the activation energy for the diffusion of the static phase-wave, T is absolute temperature, R is the gas constant, and ω'_{oo} is the frequency of fluctuation at absolute zero temperature (which should match the frequency of the conformer motions at T = 0 K). The ratio (RT/G^*_1) appearing in front of the modulus can be re-written by re-plotting the data in Figure 5.12 as a function of stress, instead of modulus, to conform to what the Eyring formula stipulates. The modulus G^* is equal to τ^*/γ where τ^* is the shear stress amplitude; so, if we plug this expression into Eq. (5.13), we now obtain $(RT/G^*_1\gamma)$ for the stress coefficient in Eq. (5.14). For instance, for the PMMA of Figure 5.12, obtained from a frequency sweep done at 2% strain: $\omega'_o = 34.1$, k = 0.5807, $(T/G^*_1) = 0.01803$, and thus $(T/G^*_1\gamma) \sim 1$. This gives an order of magnitude for the stress coefficient in Eq. (5.13).

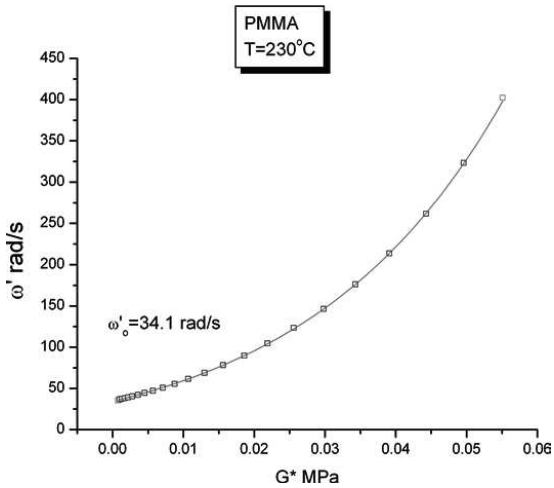

Figure 5.12 Plot of ω′ vs G* for PMMA at T = 230 °C, 2% strain. ω'_o is found by extrapolation to G* = 0. The continuous line is a fit by Eq. (5.12)

When k is different from 1, we can apply the same rewrite of Eq. (5.13) into the Eyring format but using ω'_{av} instead of ω′. We obtain:

$$\omega'_o = \omega'_{oo} \exp\left(-\frac{\Delta_{\omega'}}{RT}\right)$$

$$\omega'_{av} = \omega'_{oo} \exp\left[-\frac{\left(\Delta_{\omega'} - \left(\frac{RT}{G^*_1\gamma}\right)\tau^*\right)}{RT}\right]$$

$$\omega'_{av} = k\omega' + (1-k)\,\omega'_o \qquad (5.15)$$

In Figure 5.96, we see the split of $(G'/G^*)^2$ vs ω for a PS melt that has been submitted to a certain thermo–mechanical history prior to performing the frequency sweep done at 217.5 °C, with a strain of 30%. The frequency increases during the test, an option usually designated "an upsweep".

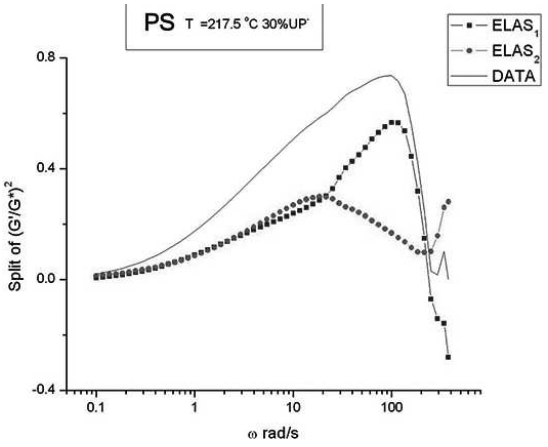

Figure 5.96 Split of $(G'/G^*)^2$ vs ω into χ_1 and χ_2 for the PS melt at T = 217.5 °C and γ = 30%

In the legend box, $ELAS_1$ and $ELAS_2$ represent χ_1 and χ_2, respectively. The $(G'/G^*)^2$ curve is also shown in the figure ("DATA"). One sees for this pre-sheared melt that both χ_1 and χ_2 rise simultaneously with ω and that χ_2 reaches a maximum at $\omega \sim$ 20 rad/s while χ_1 continues to rise, yet χ_1 itself reaches a maximum at $\omega =$ 100 rad/s before rapidly decreasing. The maxima for χ_2 and χ_1 are 0.3 and 0.6, respectively. It is interesting to see the large impact of a pre-shearing treatment of the melt (a condition called "shear-refinement") on the modification of the rheology of the dual-phases; an untreated PS melt behaves very closely to what we have analyzed for PMMA (see Figure 5.81 and Figure 5.91). The new method of analysis of viscoelastic data presented in this chapter appears quite powerful to determine what happens to shear-thinning or strain softening as a result of a given shear-refinement treatment. In Figure 5.96, from $\omega = 0.1$ to 20 rad/s, the two dual-phases are in the terminal zone, both shear-thinning incoherently. Between $\omega =$ 20 and 100 rad/s, the χ_2-phase (phase-line network) is shear-thinning coherently in the rubbery plateau, but the χ_1-phase is still incoherent. For ω between 100 and 200 rad/s, both dual-phases are stretching coherently, a condition that may have consequences for the long-term stability of the deformed state obtained. This type of experiment and analysis with the dual-phase model, we suggest, must be sys-

tematically accomplished to understand the impact of thermo–mechanical treatments, such as "rheo-fluidification", also called "disentanglement" (Chapters 2 and 4, refs [40, 41]), on the long-term stability of new states for the entanglement network.

In Figure 5.97, we study the variation of the activated strand coherence factor, k, as a function of ω for the polystyrene melt of Figure 5.25 analyzed at T = 150 °C and 2% strain. The reason for lowering the temperature is to make apparent the maximum of the melt elasticity, $\chi = (G'/G^*)^2$, within the range of frequencies studied. For ω = 0.01 to ~7 rad/s, the value of k is constant at 0.5. This range corresponds, in Figure 5.25, to the left of the maximum of $(G'/G^*)^2$, the value of k starting to deviate at exactly the value of ω for the maximum.

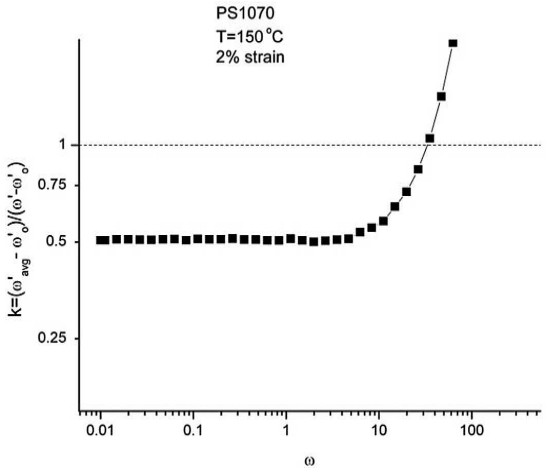

Figure 5.97 Plot of the activated strand coherence factor, k, vs ω for PS at T = 150 °C, 2% strain. Same data as in Figure 5.25

When ω is greater than 7, k quickly rises with ω and becomes 1 for ω ~ 37 rad/s. The meaning of Figure 5.97 is that k only remains constant over a restricted range of frequencies, up to the maximum of the melt elastic stored energy. The points located above the horizontal line k = 1 cannot physically be larger than 1 so that, in fact, they remain equal to 1 once k has reached this value. Eq. (5.16) controlled the mechanism of deformation while k was constant and remained valid in the regime where k increased to 1, yet is now in default for the points above the k = 1 line. We assume ,first, that Eq. (5.14) remains valid but now applies to a modulus, $G^{*(2)}$, that defines deformation in the χ_2-phase; second, that there is another com-

As said in the preamble, it is a goal of the research that led to the writing of this book to set new grounds for the understanding of polymer properties using the new concepts of grain-field statistics. Interestingly, or perhaps annoyingly for the reader, the equations describing this new open dissipative interactive systems statistics are not given explicitly in the book. This was a deliberate choice, because they are the subject of a totally different book that explores the mathematical ramifications of the original assumptions and concepts. The decision was made to remain intuitive in defining the dual-phase and cross-dual-phase systems by sketches and cartoons instead of mathematical formulas and simulations. Nevertheless, the analogies through cartoon sketches explain rather simply the interactive coupling in polymers, from the solid state to the liquid state, from flow to molecular motions, for amorphous and crystalline materials. In particular, the program of research explored in the book is set to determine how the new statistics can not only explain all the classical properties of polymers (Chapter 5) but also "sustained-orientation", which classical models cannot explain, and predict the conditions to successfully prepare "plastic battery materials", an application described below.

8.2 Industrial Applications: Improve the Processability of Existing and New Resins

The plastics industry is the source of 4% of the total worldwide energy consumption and Europe takes a share of approximately 20% of the total production of plastic materials. The industry's main problem relates to the high viscosity of molten plastics, which in turn leads to high energy consumption during processing. Large resources are invested all over the world every year to improve the processability of existing and new resins.

This book is the result of trying to understand "disentanglement technology", i.e., the development of engineering processing solutions that substantially decrease the viscosity of melts, allows them to be processed at lower temperatures, under low pressure, without or with much less degradation, and with improved dispersion when additives are compounded. By implementing "disentanglement technology" into standard and established industrial procedures, the temperature needed to process polymers can be reduced by 50–100 °C, which has a significant impact on the reduction of energy consumption to produce plastics and compounds. All these benefits of "disentanglement technology" were real, quantified, yet they were not understood; worse, they contradicted the established understanding.

It took me about 10 years of academic research to come up with a different model to explain the source of molecular motions and flow in polymers compatible with the sustained-orientation results. The driving force behind this research was not to create a new theory in polymers, it was the comprehension – against all the rejections by my peers – of practical results that allowed the processing of polymer melts at higher throughputs, with less degradation and with a lower energy cost, to obtain better and cheaper finished products. It did not take me long to realize that the key to make all these processing benefits happen was a better understanding of entanglements, its relationship to viscosity, and the understanding of viscoelasticity with respect to polymer interactions. These were the keys to open up a new world of entanglement manipulation technology to obtain, in particular, a significant reduction of the viscosity of the melt (by "disentanglement").

This new understanding of polymer interactions and entanglement expresses a paradigm shift in polymer physics that leads to a roster of new innovative applications (see Appendix A: Rheo-fluidification Markets).

The "disentanglement technology of the first generation" has already had an immense impact in specific industrial areas such as in the extrusion of plastic melts at lower temperatures with a 40% throughput increase, the increase of permeability in films for the food industry, improved dispersion of nanoparticles in polymer melts, processing under a much lower pressure and at a lower temperature with an identical throughput, increase of productivity and cost reduction for injection molding, extrusion and compounding lines, extrusion for the pharmaceutical industry, biomaterial fabrication for the medical industry (electro-spinning-writing), and the 3D printing industry etc. For instance, the high temperatures necessary for processing plastics (in extrusion or injection molding) prevent the pharmaceutical industry from incorporating temperature-sensitive active pharmaceutical ingredients into pharmaceutical grade polymers, which is a very innovative approach that has attracted significant interest in pharmaceutical technology. The new understanding of flow in entangled polymers explains how to "disentangle" melts, reduce their viscosity drastically, and process them at low temperatures to make it feasible.

Pink-Flow Technology

What I call "pink-flow" technology describes the second generation of machinery, processes, and new materials produced following this new understanding of the parameters to control the "entanglement stability" of polymer melts.

The first generation of "disentanglers" was very useful to discover "sustained-orientation" and to address its obvious immediate applications. However, the first generation machines had two problems: the first one was the necessity to increase the length of the disentangling hardware as the throughput increased. This made